Mutation of the Putative Hydrogen-Bond Donor to P_{700} of Photosystem I†

Yajing Li,‡ Marie-Gabrielle Lucas,§ Tatyana Konovalova,‡ Brian Abbott,‡ Fraser MacMillan,|| Alexander Petrenko,‡ Velautham Sivakumar,⊥ Ruili Wang,⊥ Gary Hastings,⊥ Feifei Gu,‡ Johan van Tol,# Louis-Claude Brunel,# Russell Timkovich,‡ Fabrice Rappaport,§ and Kevin Redding*,‡

Department Chemistry, University of Alabama, Tuscaloosa, Alabama 35487-0336, Institut de Biologie Physico-Chimique, 13 rue Pierre et Marie Curie, 75005 Paris, France, Department of Physical and Theoretical Chemistry, J.W. Goethe Universität, Frankfurt am Main D-60439, Germany, Department of Physics & Astronomy, Georgia State University, Atlanta, Georgia 30303, and Center for Interdisciplinary Magnetic Resonance, National High Magnetic Field Laboratory, Florida State University, Tallahassee, Florida 32310

Received December 30, 2003; Revised Manuscript Received July 27, 2004

ABSTRACT: The primary electron donor of photosystem I (PS1), called P_{700}, is a heterodimer of chlorophyll (Chl) *a* and *a*′. The crystal structure of photosystem I reveals that the chlorophyll *a*′ (P_A) could be hydrogen-bonded to the protein via a threonine residue, while the chlorophyll *a* (P_B) does not have such a hydrogen bond. To investigate the influence of this hydrogen bond on P_{700}, PsaA-Thr739 was converted to alanine to remove the H-bond to the 13^1-keto group of the chlorophyll *a*′ in *Chlamydomonas reinhardtii*. The PsaA-T739A mutant was capable of assembling active PS1. Furthermore the mutant PS1 contained approximately one chlorophyll *a*′ molecule per reaction center, indicating that P_{700} was still a Chl *a*/*a*′ heterodimer in the mutant. However, the mutation induced several band shifts in the visible $P_{700}^+ - P_{700}$ absorbance difference spectrum. Redox titration of P_{700} revealed a 60 mV decrease in the P_{700}/P_{700}^+ midpoint potential of the mutant, consistent with loss of a H-bond. Fourier transform infrared (FTIR) spectroscopy indicates that the ground state of P_{700} is somewhat modified by mutation of ThrA739 to alanine. Comparison of FTIR difference band shifts upon P_{700}^+ formation in WT and mutant PS1 suggests that the mutation modifies the charge distribution over the pigments in the P_{700}^+ state, with ∼14−18% of the positive charge on P_B in WT being relocated onto P_A in the mutant. ^{1}H-electron-nuclear double resonance (ENDOR) analysis of the P_{700}^+ cation radical was also consistent with a slight redistribution of spin from the P_B chlorophyll to P_A, as well as some redistribution of spin within the P_B chlorophyll. High-field electron paramagnetic resonance (EPR) spectroscopy at 330-GHz was used to resolve the **g**-tensor of P_{700}^+, but no significant differences from wild-type were observed, except for a slight decrease of anisotropy. The mutation did, however, provoke changes in the zero-field splitting parameters of the triplet state of P_{700} ($^3P_{700}$), as determined by EPR. Interestingly, the mutation-induced change in asymmetry of P_{700} did not cause an observable change in the directionality of electron transfer within PS1.

In higher plants and green algae, the photosynthetic reaction occurs within two large pigment−protein complexes located in the thylakoid membranes of the chloroplast: photosystems I and II (PS1 and PS2).[1] These two systems exemplify the type 1 ("iron−sulfur") and type 2 ("quinone") reaction centers, respectively, based on their terminal electron acceptors. In oxygenic phototrophs, PS2 and PS1 act in tandem to oxidize water and reduce $NADP^+$, but there are several anoxygenic photosynthetic bacteria that use only one type of reaction center protein.

All known reaction centers share a similar structural motif with a core of reaction centers composed of two similar or identical integral membrane subunits, to which the various redox cofactors are bound. Both the protein structural motifs and the cofactor arrangements are characterized by a pseudo-C_2 symmetry axis, giving rise to two similar branches of cofactors. The overall structural arrangement of the cofactors in reaction centers is (1) the primary electron donor, which is a chlorophyll (Chl) dimer placed along the symmetry axis with the planes of the two chlorin rings parallel, (2) the primary electron acceptor, also a chlorin, and (3) a quinone. In type 1 reaction centers, an Fe_4S_4 cluster located along the symmetry axis is the next electron acceptor; two more Fe_4S_4 clusters located on a peripheral subunit serve as terminal acceptors. Charge separation in type 2 reaction centers is known to proceed unidirectionally down only one

† This work was supported by a DOE Energy Biosciences Grant (No. DE-FG02-00ER15097) and an NSF CAREER award (MCB-0347935) to K.R. G.H. acknowledges support from the USDA (Grant No. 35318-10894). F.M. was supported by an EU Marie-Curie Fellowship (Grant ERBCHRXCT940524) and the DFG (Grant SFB472).

* To whom correspondence should be addressed. Mailing address: Departments of Chemistry and Biological Sciences, University of Alabama, Tuscaloosa, AL 35487-0336. Phone: (205)348-8430. Fax: (205)348-9104. E-mail: Kevin.Redding@ua.edu.

‡ University of Alabama.

§ Institut de Biologie Physico-Chimique.

|| J. W. Goethe University.

⊥ Georgia State University.

National High Magnetic Field Laboratory.

[1] Abbreviations: BChl, bacteriochlorophyll; Chl, chlorophyll; ENDOR, electron-nuclear double resonance; EPR, electron paramagnetic resonance; FTIR, Fourier transform infrared; hfc, hyperfine coupling; HF-EPR, high-field (frequency) EPR; P_A, chlorophyll *a*′ on A-side of P_{700}; P_B, chlorophyll *a* on B-side of P_{700}; PhQ, phylloquinone; PS1, photosystem I; PS2, photosystem II; RC, reaction center; WT, wild-type.

10.1021/bi036329p CCC: $27.50
Published on Web 00/00/0000 PAGE EST: 13.1

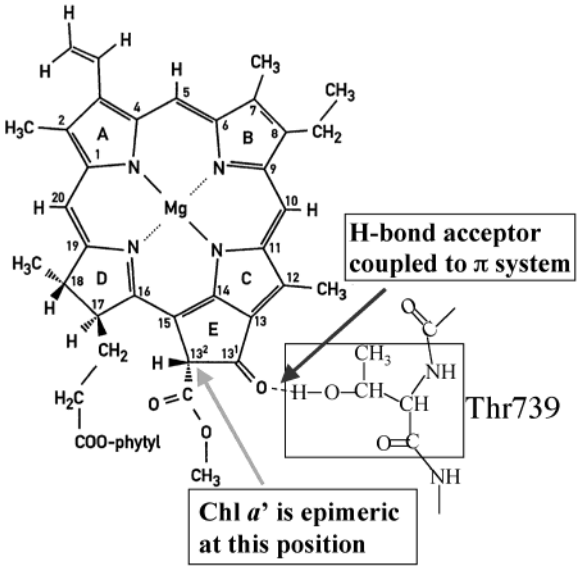

FIGURE 1: Structure of chlorophyll *a*. The Chl *a*′ epimer has the alternate stereochemistry at position 13^2. The H-bond donated by PsaA-Thr739 is also indicated.

of the branches (*1*, *2*), which likely reflects the functional difference between the two quinones in these reaction centers: one is an intermediate in electron transfer, and the other is a terminal acceptor.

Photosystem I is the best-characterized type 1 reaction center. The crystal structure of PS1 at 2.5-Å resolution reveals that 12 protein subunits (PsaA to PsaF, PsaI to PsaM, and PsaX), 96 Chl *a* molecules, 22 carotenoids, 2 phylloquinone (PhQ) molecules, and 3 Fe_4S_4 clusters are present (*3*). The core of PS1 is a heterodimer of the two large subunits, PsaA and PsaB, which are 45−50% identical in their sequence and are similar in their tertiary structure. PsaA and PsaB each contain 11 transmembrane α-helices (*4*, *5*). The six N-terminal α-helices bind a large number of chlorophyll *a* molecules and carotenoids, the role of which is to harvest photons and transfer excitation energy to the reaction center. The five C-terminal α-helices form two interlocking semicircles holding all of the electron-transfer cofactors in the lipid bilayer region. The cofactors in order are as follows: P_{700}, a special pair of chlorophylls; a pair of Chl *a* molecules (ec2 and ec3); a PhQ; F_X, an Fe_4S_4 cluster. The terminal electron acceptors, F_A and F_B, are bound by the extrinsic subunit PsaC on the stromal side (*6*).

Surprisingly, the 2.5-Å resolution crystal structure of PS1 from *Thermosynechococcus elongatus* (*3*) revealed that P_{700} is not a Chl *a* dimer, as had been assumed. While P_B is a Chl *a*, P_A is a Chl *a*′, the 13^2-epimer of Chl *a* (see Figure 1). The side chain of a threonine residue (PsaA-Thr743) is in a favorable position to donate a hydrogen bond to the 13^1-keto oxygen. The hydroxyl group of this threonine residue also seems to participate in a H-bonding network involving a bound water molecule, which donates a H-bond to the 13^2-methyl ester oxygen of P_A. This water has another three potential hydrogen partners around it: hydroxyls of PsaA-Ser607 and PsaA-Tyr603 and the backbone oxygen of PsaA-Gly739. However, P_B has no comparable H-bond network. Thus, P_{700} is fundamentally asymmetric, and the H-bond to the 13^1-keto oxygen would seem to be the most important functional feature of this asymmetry, since this keto group is part of the conjugated π system. These structural features would seem consistent with electron-nuclear double resonance (ENDOR) measurements of P_{700}^+ that estimated a ≥5:1 localization of spin on P_B compared to P_A (ref *7* and references therein). However, ($P_{700}^+ - P_{700}$) Fourier transform infrared (FTIR) difference spectra have been interpreted in terms of a model in which the positive charge is shared equally between the two Chls (*8*).

Symmetry and asymmetry play an important part in overall electron transfer through PS1. Recently, evidence was obtained for the use of both potential electron-transfer branches (*9*). Electron transfer from the PhQ to F_X is biphasic with the time constants of ∼20 and ∼200 ns (*9*−*13*). Mutation of a tryptophan near each PhQ resulted in alteration of both the rate and spectrum of a specific kinetic component, allowing identification of PhQ_A as the "slow quinone" and PhQ_B as the "fast quinone" (*9*). The relative amplitudes of these two components (assuming the same extinction coefficient at 380 nm) was about 35% fast and 65% slow, which may represent the fraction of electrons taking the B and A branches, respectively. Thus, the symmetrical structure of PS1 would allow electron transfer down both branches, but asymmetry between the PhQ sites would allow for different rates of electron transfer to F_X. It is possible that asymmetry within the primary donor might play a role in determining the relative use of the two branches. Photosystem I thus presents an interesting intermediate case between type 2 reaction centers, in which electron transfer is unidirectional, and the homodimeric type 1 reaction centers of green sulfur bacteria and heliobacteria (*14*, *15*), in which the two branches are indistinguishable.

To examine the role of the H-bond donor to the 13^1-keto oxygen of P_A, we mutated this threonine (PsaA-Thr739) to alanine in *Chlamydomonas reinhardtii*. The PsaA-T739A mutation has a striking effect upon the $P_{700}^+ - P_{700}$ difference spectra in the visible and infrared. We used electron paramagnetic resonance (EPR) spectroscopy at high magnetic field and electron-nuclear double resonance (ENDOR) spectroscopy to characterize the effects of the mutation upon the electronic structure of P_{700}^+. We also wished to test the hypothesis that the H-bond may allow enolization of Chl *a*, facilitating its conversion to Chl *a*′ in situ (*7*). The analysis of a larger set of substitution mutants at this site (to histidine, tyrosine, and valine) in the same species by Witt et al. (*16*) has been published, and our results largely agree with theirs. However, as discussed in more detail below, the effects of the substitution by alanine seem to be even more severe than any of these previously described mutations.

EXPERIMENTAL PROCEDURES

Site-Directed Mutagenesis. The point mutation was introduced by a three-stage polymerase chain reaction (PCR)-based mutagenesis technique (*17*) using oligonucleotides beyond the restriction sites flanking the desired mutation to amplify the PCR products. The PCR products were cloned directly into the corresponding plasmids using the same restriction sites. The plasmids include the *psaA-3* gene, along with flanking sequences to direct homologous recombination and a bacterial *aadA* gene, which was used as a selectable marker (*18*). After it was sequenced to confirm the point mutations, the plasmid DNA was coated onto 1-μm diameter gold particles and introduced into algae chloroplast

ballistically. The recipient strain of *C. reinhardtii* was KRC91 (*P71 FUD7 psaA*Δ), which have no PS2 due to the *FUD7* mutation (*19*) and less antenna background due to the P71 mutation (J. Girard-Bascou, personal communication), to simplify PS1 purification for biophysical analyses. These strains were generated in the same way as the recipient strains used in ref *20*; the *P71* mutant was a kind gift from Jacqueline Girard-Bascou (Institut de Biologie Physico-Chimique, Paris). Transformants were selected by resistance to the antibiotics spectinomycin and streptinomycin. The mutations within the transformants were confirmed by PCR using purified genomic DNA as the template. The control strain (wild-type) KRC1003 was made by crossing a *nac2* strain (*21*) with a *P71* strain to create a *nac2 P71* double mutant, containing no PS2 and lowered amounts of light-harvesting complexes.

Preparation of Thylakoid Membrane and PS1 Particles. The cells were grown in Tris−acetate−phosphate (TAP) medium (*22*) at 25 °C in light. Thylakoid membranes were prepared by sucrose-gradient centrifugation as previously described (*23*). For preparation of PS1 particles, the membranes were suspended at a chlorophyll concentration of 150 μg/mL in a buffer containing 50 mM Tricine (pH 8), 1 mM EDTA, 1 mM aminocaproic acid, and 1 mM benzamidine. One part of 10% dodecyl-β-D-maltoside (β-DM) was added to 8 parts of thylakoid suspension, and the mixture was rotated gently in the dark for 40 min on ice. After centrifugation at 15 000 × *g* for 15 min to remove nonsolubilized material, the supernatant was collected and diluted at ∼1:10 ratio with TED buffer (10 mM Tricine, pH 8, 1 mM EDTA, 0.04% β-DM, 10 mM $MgSO_4$). PS1 particles were collected by centrifugation at 50 000 × *g* for 3 h. PS1 pellets were resuspended and homogenized in TED + 20% glycerol and were stored at −80 °C. All steps were performed in low light and in the cold (0−4 °C). Chlorophyll concentration was determined in 80% acetone extracts (*24*).

Cofactor Analysis of PS1 Particles. PS1 particles (40 μg of Chl *a*) were extracted by addition of 2 volumes of degassed ethyl acetate followed by vortexing and sonication in an ice−water bath for 2 min. After a 2-min centrifugation at 15 000 × *g*, the upper organic phase was removed. To make the extraction quantitative, the aqueous phase was reduced as much as possible, another volume of ethyl acetate was added, and the extraction was repeated. After this, the protein-containing pellet was white, and all green material was present in the organic phase. The ethyl acetate extracts were joined and passed through a 0.4-μm Millex-FH filter, concentrated with a stream of nitrogen gas to a volume of 20−30 μL, and separated by HPLC, based on the method of Nakamura and Watanabe (*25*). A Partisil ODS-3 column (250 mm × 4.6 mm, 5μ) from Alltech was used for the separation, and samples were eluted with acetonitrile/methanol/ethanol/water (85:9:3:3). The material exiting the column was monitored at 663 nm for maximum sensitivity and selection of Chl *a* and *a*′. Chlorophyll *a* and *a*′ eluted at 9.2−9.4 and 10.4−10.6 min, respectively. They were collected separately, dried down with a stream of nitrogen gas, dissolved in a minimum volume of acetonitrile, and loaded onto the C-18 column again for quantification of the peaks. Purified Chl *a* was purchased from Sigma for use as a standard. This was partially converted to Chl *a*′ by treatment with base in the light, and the elution positions of Chl *a* and Chl *a*′ were determined; these were very similar to those previously reported (*25*). The identity of the eluted molecules was confirmed by UV/visible spectroscopy and mass spectrometry (data not shown).

FTIR Difference Spectroscopy. PS1 membranes or particles were suspended in Tris buffer (pH 8). The PS1 membranes or particles were pelleted and placed between a pair of rectangular CaF_2 windows separated by Teflon spacers. No mediators were added for the spectra presented here, but mediator addition resulted in identical spectra. FTIR difference spectra were recorded using a BRUKER IFS/66 FTIR spectrometer. Light-minus-dark and dark-minus-dark FTIR difference spectra were constructed as described previously (*26, 27*) using continuous illumination from a helium neon laser (632.8 nm). All measurements were conducted at room temperature.

Redox Potential of P_{700}. Redox titrations were performed in an electrochemical cell as described previously (*28*). The gold grid used as a working electrode was modified with pyridine-3-carboxaldehydethiosemicarbazone to avoid irreversible protein adhesion. The cell was filled with membranes resuspended in 20 mM *N*-2-hydroxyethylpiperazine-*N*′-2-ethanesulfonic acid (Hepes) (pH 7.2), 50 mM KCl, and redox mediators at a concentration of 50 μM (ferrocene carboxylic acid, ferricyanide, *N*,*N*-dimethyl-*p*-phenylenediamine, 1,1-dimethylferrocene, or *N*,*N*,*N*,*N*-tetramethyl-*p*-phenylenediamine). At each potential, the photoinduced absorption changes were measured 1 ms after the flash.

Optical Spectroscopy in Vitro. PS1 particles were diluted to ∼10 μM Chl in a buffer containing 50 mM Hepes (pH 7.5), 40 mM KCl, 5 mM $MgCl_2$, 1 mM sodium ascorbate, and 1 μM phenazine methosulfate. The absorption changes due to the photooxidation of P_{700} were recorded using a CARY double-beam spectrophotometer equipped with a light-emitting diode (LED) system to illuminate the sample cuvette; appropriate filters were used to block the actinic light from reaching the detectors.

Optical Spectroscopy in Vivo. Spectroscopic measurements in whole cells were performed using a home-built spectrophotometer (*29*). The absorption changes were probed by using short monochromatic flashes. A Nd:YAG pumped optical parametric oscillator (Opotek) produced the monochromatic flashes in the 405−500 nm range. A tunable dye-laser pumped by the second harmonic of a Nd:YAG laser was used to excite the sample at 700 nm. The high signal-to-noise ratio of the spectrophotometer (10^5) when using the samples with high optical densities, such as cell suspensions, and the time resolution (5 ns) of the technique have been described (*30*). *C. reinhardtii* cells were grown in TAP medium at 25 °C under low light (6 $\mu E \cdot m^{-2} \cdot s^{-1}$) and then resuspended in 20 mM Hepes (pH 7.2) containing 20% (w/v) Ficoll and 5 μM carbonyl cyanide (4-(trifluoromethoxy) phenyl) hydrazon (FCCP) to collapse the permanent electrochemical proton gradient. The decay-associated spectra (DAS) of the kinetic phases were obtained from a global analysis of the individual kinetics obtained at each wavelength, as described previously (*9*)

EPR and ENDOR Spectroscopy. PS1 particles (1−1.5 mg/mL Chl) were put in standard 4-mm Suprasil quartz EPR tubes and illuminated for ∼10 s and then frozen at 77 K while under illumination from a white 200 W lamp passed through a 20-cm water filter. X-band EPR and ENDOR

spectra of P_{700}^+ in these samples were measured by standard techniques on a Bruker ESP 300E EPR spectrometer equipped with a DICE ENDOR ESP 350 system and a Bruker ER4111 temperature controller. For high-field EPR, samples were generated by a similar method but in the presence of ferricyanide. W-band (95 GHz) spectra were performed with a Bruker ELEXSYS E600 EPR spectrometer. Spectra were also measured at a frequency of ~330 GHz and fields near 11.6−11.7 T, using a P-doped Si chip as internal standard, as previously described (*31*).

For triplet measurements, thylakoid membranes were treated with 7 M urea for 1 h on ice to remove PsaC (*32*), followed by addition of 50 mM $MgSO_4$ and centrifugation. They were washed with an equal volume of 20 mM Tricine (pH 8.0), centrifuged again, and resuspended with a minimal volume. One hundred microliters of treated membranes were transferred to a degassed 4-mm EPR tube containing 10 μL of 0.55 M $Na_2S_2O_4$ in 1 M glycine (pH 10). After 30 min at room temperature in the dark, they were illuminated for 10 min in an ice−water bath to double-reduce the phylloquinone(s). EPR spectra of $^3P_{700}$ were taken at 5 K with illumination of the cavity; background spectra were taken in the dark and under the same conditions.

Theoretical Modeling and DFT Calculations. Intermolecular distances and relative orientations of P_{700} Chls and nearby amino acid residues were taken from the X-ray structure of *T. elongatus* PS1 (*3*). The first model complex included the P_{700}^+ radical cation and the amino acid residues PsaA-Thr743 (H-bond donor to P_A), PsaA-His680 (axial ligand to P_A), and PsaB-His660 (axial ligand to P_B). To limit the size of the model complexes, the phytyl tails of P_A and P_B were each replaced with a methyl group. In addition, for each amino acid residue, the N-terminal peptide (−CO−NH−Cα) was converted to an amine (H−NH−Cα) and the C-terminal peptide (Cα−CO−NH−) was converted to an aldehyde (Cα−CO−H). Hydrogen atoms were added using modeling facilities of the HyperChem 7 program package (Hypercube Inc., Gainesville, FL). To create the second model complex, the first model structure was modified by converting the side chain of PsaA-Thr743 to a methyl group using the modeling facilities of HyperChem.

Density functional calculations of these complexes were performed using Gaussian 98 (Gaussian Inc., Pittsburgh, PA) installed on a CRAY SV1 computer at the Alabama Supercomputer Center. The B3LYP hybrid functional was used in combination with 3-21G Gaussian basis set. This basis set was used for these very large molecular complexes to reduce computation time to a reasonable amount. Preliminary calculation of isotropic hfc's of model complexes of individual chlorophyll *a* radical cation with different amino acid residues has shown a reasonable agreement between parameters calculated in 3-21G and the 6-31G(d) basis sets (Petrenko, unpublished results). The B3LYP 6-31G(d) basis set was successfully used in previous calculations of the spin density distribution and hyperfine coupling constants of individual chlorophyll cations (*33*). (Unlike the EPR-II basis set, magnesium is supported by the 6-31G(d) and 3-21G basis sets.)

RESULTS

Assembly of Photosystem I in the PsaA-T739A mutant. The codon for PsaA-Thr739 was converted to an alanine codon and reintroduced into a strain lacking the third exon of the *psaA* gene (*34*). The mutant strain accumulated PS1 to similar levels as the WT control strain and could grow photoautotrophically like the WT strain (data not shown). Thylakoid membranes prepared from this strain had the normal complement of PsaA, PsaD, and PsaF polypeptides, as judged by quantitative immunoblot analysis (data not shown).

Cofactor Analysis of PsaA-T739A. P_{700} in *T. elongatus* PS1 is a Chl *a*′/Chl *a* heterodimer (*3*) and Chl *a*′ has been observed in every oxygenic species examined with an abundance consistent with one Chl *a*′ per PS1 RC (*25*, *35*, *36*). It has been suggested that conversion of Chl *a* to Chl *a*′ may occur in situ with the assistance of the H-bond donor (*37*). Therefore, it was of interest to know whether PS1 in PsaA-T739A still contained Chl *a*′. We first ascertained that WT PS1 from this species contained Chl *a*′. Our attempts to extract and measure Chl *a*′ from *Chlamydomonas* preparations using the procedure of Nakamura and Watanabe (*25*) proved unsuccessful, in that we obtained far more Chl *a*′ than expected—usually three to five Chl *a*′ per 100 Chl *a* in the best cases (data not shown). Although buffering the solution at pH 8 before extraction helped, it did not completely eliminate isomerization. We developed a new procedure involving extraction with ethyl acetate, allowing a rapid two-phase separation. Chlorophyll partitions completely into the organic phase, rapidly removing it from water, which is probably key to preventing isomerization at position 13[2]. Using this procedure (described in detail in the Experimental Procedures), we were able to observe one Chl *a*′ per 120 Chl *a* in PS1 from *Synechocystis* PCC6803 (data not shown), convincing us that the procedure did not provoke significant postextraction isomerization. In WT PS1 from *C. reinhardtii* (from the same background as the mutant), we obtained one Chl *a*′ per 130−150 Chl *a* in two different preps. In PS1 from the PsaA-T739 mutant, we obtained one Chl *a*′ per 150−170 Chl *a* in two different preps (Figure 2). Therefore, we conclude that loss of PsaA-Thr739 does not block incorporation of Chl *a*′ in *C. reinhardtii* PS1. Assuming, as seems likely, that the Chl *a*′ that we observe after extraction is part of P_{700}, as it is in *T. elongatus*, then P_{700} in the PsaA-T739A mutant is still a Chl *a*′/Chl *a* heterodimer, contrary to the prediction of Webber and Lubitz (*7*).

(P_{700}^+ − P_{700}) FTIR Difference Spectra. Vibrational spectroscopy has been widely used to study the interactions of the primary chlorophyll donor (P_{700}) of PS1 with the protein (*8*, *26*). Using light-minus-dark FTIR difference techniques, one can aquire a spectrum associated with the ground state and the oxidation of P_{700}. The FTIR difference spectrum is sensitive to small structural changes of chlorophyll in its local environment and to changes in H-bond strengths (*38*, *39*). Figure 3 shows the P_{700}^+ − P_{700} FTIR difference spectra obtained using wild-type (top) and PsaA-T739A mutant (middle) PS1 particles. The difference between these two spectra is also shown (bottom, black line), along with the double difference spectrum (DDS) obtained using thylakoid membranes (bottom, gray line). The FTIR DDS obtained using membranes or particles are very similar, indicating that the detergent treatment used for isolation of PS1 particles does not result in any molecular perturbations of the P_{700} pigments or the immediate protein environment.

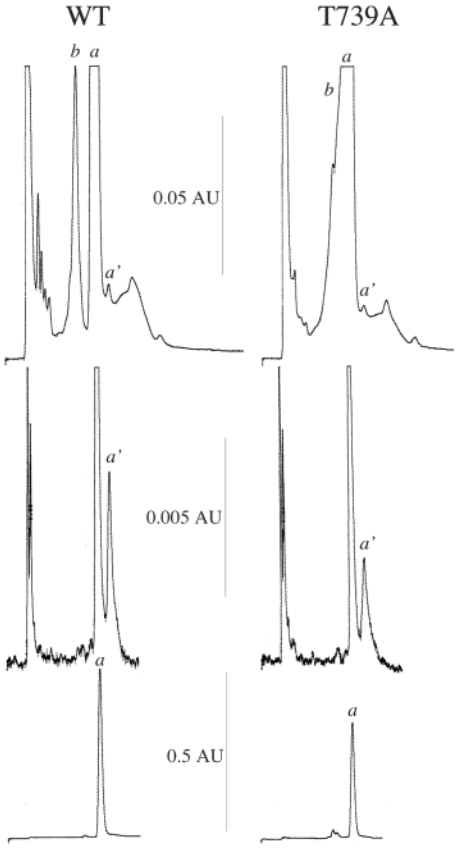

FIGURE 2: HPLC analysis of Chl *a* and *a*′ content in PS1 from WT and the PsaA-T739A mutant. The top row shows the HPLC traces (at 663 nm) of ethyl acetate extracts of PS1 from WT and PsaA-T739A (full scale = 0.1 AU). The Chl *a* and Chl *a*′ fractions were collected separately. The middle row is the injection of the Chl *a*′ fraction (full scale = 0.01 AU). The Chl *a* contaminating it (due to tailing) was collected separately and added to the Chl *a* fraction, which was then injected (bottom row; full scale = 1 AU). Peaks assigned to Chl *b*, Chl *a*, and Chl *a*′ are indicated.

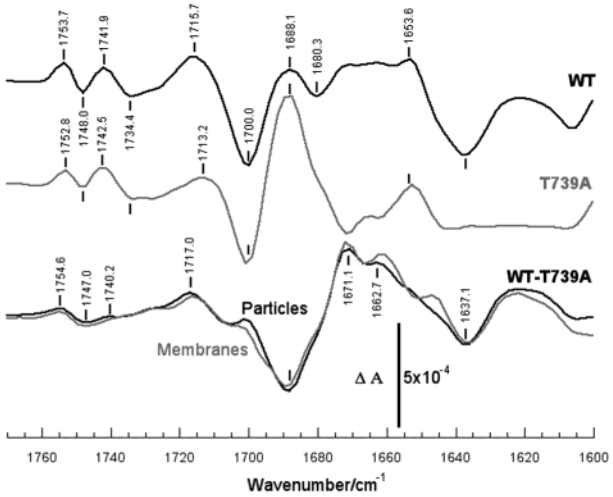

FIGURE 3: $P_{700}^+ - P_{700}$ FTIR difference spectra in 1780−1600 cm^{-1} region, obtained using WT (top) and mutant (middle) PS I particles. The WT − T739A FTIR DDS is also shown (bottom). The WT − T739A FTIR DDS obtained using thylakoid membranes is shown overlaid (bottom, gray).

In FTIR DS, positive bands originate from molecular modes associated with the P_{700}^+ state, while negative bands originate from molecular modes associated with P_{700} (ground state). Several dissimilarities are observed in the WT and mutant FTIR DS. For WT, positive bands are observed at 1654, 1688, 1716, 1742, and 1754 cm^{-1}, and negative bands are observed at 1637, 1680, 1700, 1734, and 1748 cm^{-1}. For the mutant, the negative band at 1637 cm^{-1} is modified considerably, and the positive band at 1716 downshifts to 1713 cm^{-1}. It is not clear whether the 1654(+) cm^{-1} band of WT is shifted; however, a positive band is observed at 1652 cm^{-1} in the mutant. The band at 1688 cm^{-1} could be shifted slightly, but its intensity appears to increase dramatically in the mutant.

For WT PS1, the 1734(−)/1742(+) and 1748(−)/1754(+) cm^{-1} difference bands have been assigned to an upshift of the 13^3 ester C═O's of P_A and P_B, respectively, upon cation formation (*8, 26*). The higher frequency ester C═O mode is most likely to be free of H-bonding. The 1748(−)/1754(+) cm^{-1} difference band is therefore assigned to the 13^3 ester C═O of P_B, while the 1735(−)/1741(+) cm^{-1} difference band is assigned to 13^3 ester C═O of P_A, which is involved in H-bonding to a water molecule (*3*).

The negative bands at 1748(−) and 1735(−) cm^{-1} appear to be little impacted by the PsaA-T739A mutation, while the positive bands at 1754(+) and 1741(+) cm^{-1} appear to downshift <1 cm^{-1} and upshift <1 cm^{-1}, respectively. The downshift of the ester C═O band of P_B^+ is especially prominent, giving rise to the positive band at 1755 cm^{-1} in the FTIR DDS of both the membranes and the isolated particles. Thus, in WT PS1, the 13^3 ester C═O mode of P_B absorbs at 1748 cm^{-1} and upshifts 5.7 cm^{-1} upon cation formation. In the T739A mutant, the 13^3 ester C═O mode of P_B^+ is downshifted <1 cm^{-1} relative to that of WT. The shift is not well resolved in Figure 3, because it has a magnitude that is below the instrumental resolution. However, from spectra collected at higher resolution, it was found that the 13^3 ester C═O mode of P_B absorbs at 1748.2 cm^{-1} and upshifts 4.9 cm^{-1} upon cation formation. In the T739A mutant, the 13^3 ester C═O mode of P_B^+ is downshifted 0.7 cm^{-1} relative to that of WT (*40*).

If it is assumed that the cation-induced difference band upshift is linearly related to the amount of charge on a pigment, then the 4.9 cm^{-1} cation-induced upshift and the 0.7 cm^{-1} mutation-induced downshift would indicate that the charge on P_B in the mutant is 14.3% (0.7/4.9) less than that of WT. The mutation-induced upshift of the 1741.9(+) cm^{-1} band (Figure 3) points to the suggestion that the charge on P_B^+ is relocated onto P_A in the mutant. From spectra collected at higher resolution, it is found that the 13^3-ester C═O mode of P_A upshifts 7.1 cm^{-1} upon cation formation. In the mutant, the 13^3-ester C═O mode of P_A^+ is downshifted 1.3 cm^{-1} relative to that of WT (*40*). This could indicate that the charge on P_A^+ in the mutant is 18.3% (1.3/7.1) greater than in WT. Although the above estimates of mutation-induced charge redistribution are rather crude, we do point out that a charge redistribution between P_A and P_B is by far the most likely explanation for the observed mutation-induced bandshifts (*40*).

The similarity in the FTIR DDS for PS1 membranes and particles indicate that the same hypothesis is appropriate for both membranes and particles and that detergent-induced spectral shifts can be excluded as possible contributors to the spectra. The spectra in Figure 3 also indicate that it is appropriate to compare spectra obtained using PS1 membranes or particles. It is of note that the bands due to the 13^3

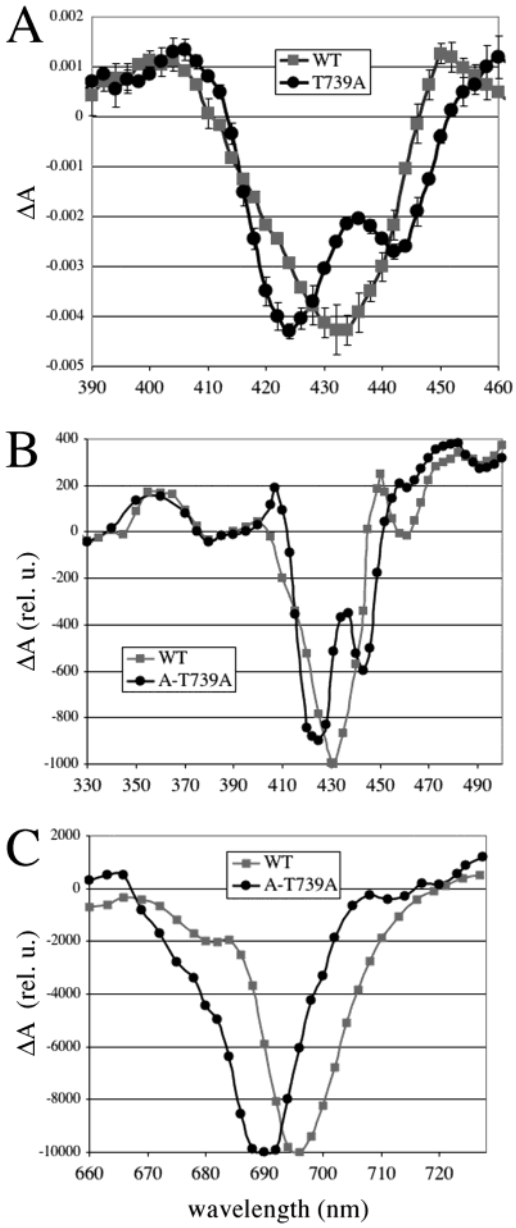

FIGURE 4: ($P_{700}^+ - P_{700}$) optical difference spectra. (A) light-minus-dark difference spectra of PS1 particles in the 390−460 nm region taken with a double-beam spectrophotometer in ascorbate and PMS; illumination was provided by red LEDs with suitable filters to remove actinic light; (B) the decay-associated spectra assigned to rereduction of P_{700}^+ in the blue region, as measured by pump−probe laser-flash spectroscopy in vivo (see Figure 9); (C) the oxidized-minus-reduced spectrum of PS1 in the red region; difference spectra of laser flash-induced absorbance changes were taken under reducing and oxidizing conditions (see Figure 5). WT is represented by gray squares; PsaA-T739A is represented by black circles.

ester C═O modes of P_A and P_B in the ground state are hardly affected by the T739A mutation. We therefore conclude that the water molecule is likely still present and possibly still H-bonded to the 13^2-ester oxygen of P_A. The assignment of the other bands in the FTIR DS is somewhat controversial. However, all of the changes can be rationalized within the framework of a mutation-induced charge redistribution, in which some positive charge on P_B is relocated onto P_A (*40*).

Optical Difference Spectra ($P_{700}^+ - P_{700}$). Absorbance difference spectroscopy was used to investigate optical features of the primary donor. In Figure 4A, the light-minus-dark difference spectra of PS1 particles from the WT and PsaA-T739A strains are shown. The optical spectrum in the blue region shows a major bleaching band centered at 432 nm in WT, corresponding to the Soret band of Chl *a* (Figure 4A). There is also a shoulder positioned at 420 nm with weak intensity. However, two bleaching bands were resolved in the mutant, the major one centered at 424 nm and a minor band centered at 442 nm. The $P_{700}^+ - P_{700}$ difference spectra over a larger spectral range in the blue region were obtained independently as the decay-associated spectra of the 4-μs component assigned to rereduction of P_{700}^+ by predocked plastocyanin in vivo (*9*). As shown in Figure 4B, there is very good agreement between the in vitro results obtained with detergent-solubilized particles and results obtained in vivo with whole cells.

The optical spectrum in the red (Q_y) region corresponds to the transition from the ground state to the lowest excited state. The major bleaching band of P_{700} in the red is centered at 696 nm in the wild-type PS1, and a band with weaker intensity is located at ∼680 nm (Figure 4C), in excellent agreement with previous results obtained with PS1 from this species (*18, 41*). In the PsaA-T739A mutant, the major bleaching band was blue-shifted to 690 nm; there was at least one additional bleaching band at ∼675−680 nm, but it was difficult to tell how many (Figure 4C). The intensity of the ∼680-nm band was somewhat variable and usually larger in particles (data not shown); it may contain contributions from bleached antenna chlorophylls. These results are in good agreement with those obtained previously by Witt et al. (*16*) in both spectral regions. However, we note that the additional bleaching band at ∼678 nm is smaller in our mutant than in any of theirs. Because the relative size of this band seems to decrease from the T739Y to the T739V mutant (*16*), it may be related to the strength of hydrogen bonding to P_A. This is consistent with the claim that the T739A mutant has the most severe effect (see below).

Redox Midpoint Potential of P_{700}. The energy difference between the ground state and the oxidized state of P_{700} can be determined by measuring its redox potential. The midpoint potential of P_{700}^+/P_{700} is at least 200 mV lower than that of Chl a^+/Chl *a* in organic solvent (*42*), most likely due to the arrangement of the two Chl molecules and their interaction with the protein. Therefore, it was of interest to see the effect caused by mutation of the hydrogen bond donor to P_A. The yield of P_{700} bleaching caused by a laser flash in thylakoid membranes was measured at a range of ambient redox potentials. The midpoint potential of P_{700}^+/P_{700} in the PsaA-T739A mutant was found to be +390 mV (Figure 5), which is 60 mV lower than that measured in WT. Thus, P_{700}^+ is less oxidizing in the PsaA-T739A mutant. Note that this shift is about twice that seen in the most severe mutant analyzed by Witt et al. (*16*), the T739V mutant.

Multifrequency EPR and ENDOR Spectra of $P_{700}^{+\bullet}$. Light-induced oxidation of P_{700} produces the $P_{700}^{+\bullet}$ cation radical. We analyzed the oxidized primary donor ($P_{700}^{+\bullet}$) within PS1 from WT and PsaA-T739A by multifrequency EPR and ^{1}H-ENDOR spectroscopy in frozen solution. The EPR spectra of $P_{700}^{+\bullet}$ produced in thylakoid membranes from the WT and PsaA-T739A mutant at X-band (9.4 GHz) and W-band (94 GHz) frequencies were unresolved Gaussian envelopes with $g = 2.0028$ (data not shown), indicating no major changes in the electronic structure of $P_{700}^{+\bullet}$ between the

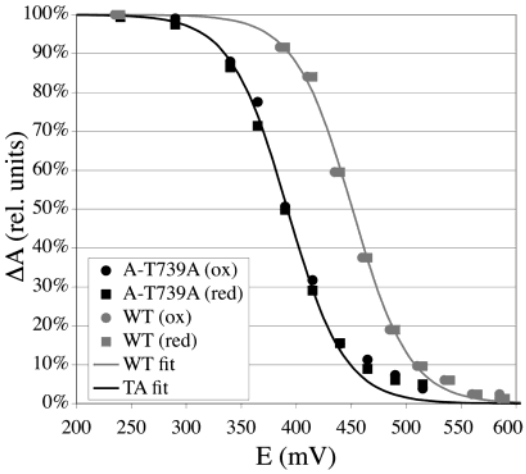

FIGURE 5: Redox titration of P_{700} in thylakoid membranes of WT (gray symbols) and PsaA-T739A (black symbols). The amplitude of the laser flash-induced bleaching in the red region (696 or 690 nm for the wild-type or mutant) was measured at various redox potentials, as described in Experimental Procedures. Circles and squares indicate data taken during the rise and the subsequent drop in redox potential, respectively; the lines are the fit to the data assuming a one-electron oxidation−reduction.

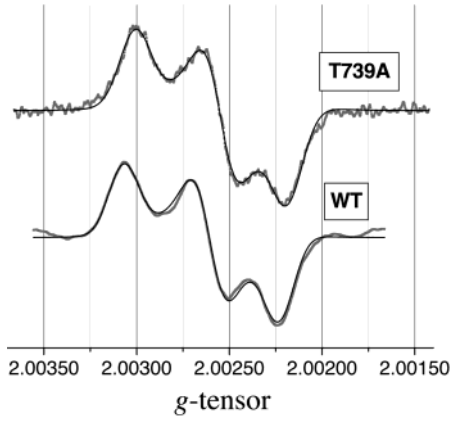

FIGURE 6: High-field EPR spectra of the P_{700}^+ cation radical in WT and the PsaA-T739A mutant, taken at a frequency of ~330 GHz. Spectra are shown as gray lines; simulations of the spectra are overlain in black. In both cases, the magnetic field was calibrated with an internal standard (P/Si; see Experimental Procedures).

Table 1: Components of the **g**-Tensor of P_{700}^+ in WT PS1 and the PsaA-T739A Mutant

form	g_{xx}[a]	g_{yy}[a]	g_{zz}[a]	$g_{xx} - g_{zz}$[b]	$g_{xx} - g_{yy}$[b]	$g_{yy} - g_{zz}$[b]
WT	2.003 09	2.002 63	2.002 26	837	468	369
PsaA-T739A	2.003 01	2.002 55	2.002 20	803	459	344

[a] Absolute experimental error = $\sim 5 \times 10^{-5}$. [b] The difference ($g_{ii} - g_{jj}$) is multiplied by a factor of 10^6. Relative error = $\sim 10^{-5}$.

mutant and the wild-type. The anisotropy of the **g**-tensor of the $P_{700}^{+\bullet}$ cation radical can be resolved at magnetic fields of 11.6−11.7 T and frequencies of ~330 GHz (*31*). At such high frequencies, the field-dependent **g**-anisotropy dominates the spectrum and the three principal components of the **g**-tensor can be determined (Figure 6 and Table 1). The **g**-tensor of $P_{700}^{+\bullet}$ in the PsaA-T739A mutant is very similar to that in the WT, although it is slightly less anisotropic (Table 1).

ENDOR spectroscopy probes the electronic structure of $P_{700}^{+\bullet}$ in a different way. Figure 7 compares the ^{1}H-ENDOR spectra obtained for $P_{700}^{+\bullet}$ in WT and PsaA-T739A. Our

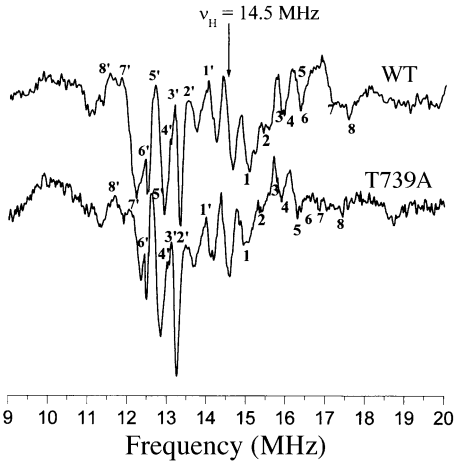

FIGURE 7: ENDOR spectra of $P_{700}^{+\bullet}$ of wild-type (upper) and mutant PsaA-T739A (lower). The Larmor frequency of ^{1}H is indicated by an arrow at 14.5 MHz. See Table 2 for assignment of the indicated lines. Conditions for spectra were T = 120 K, modulation frequency = 12.5 kHz, modulation amplitude = 2 G, microwave power = 20 mW, gain = 10^5, and time constant = 81.9 ms; 89 scans were summed.

Table 2: Proton Hyperfine Couplings (MHz) of the Wild-Type and the Mutant PsaA-T739A

		2-methyl			7-methyl			12-methyl		
group	2nd Chl	$A_\perp$	$A_\parallel$	A_{iso}[a]	$A_\perp$	$A_\parallel$	A_{iso}[a]	$A_\perp$	$A_\parallel$	A_{iso}[a]
lines[b]	1′/1	2′/2	3′/3	5′/5		4′/4	6′/6		7′/7	8′/8	
WT	0.86	1.81	2.61	3.43	2.88	2.87	3.89	3.21	5.02	5.91	5.32
T739A	0.83	1.69	2.56	3.41	2.84	2.84	3.87	3.18	4.49	5.38	4.79

[a] The isotropic hfc's (A_{iso}) were calculated using the standard formula: $A_{iso} = (2A_\perp + A_\parallel)/3$. [b] See Figure 7 for the lines in the experimental spectra.

spectra are very similar to those of Käss and Lubitz (*43*, *44*), and we have made use of their assignments here. Line pairs 1′/1 and 2′/2 were assigned to P_A, which is believed to possess low unpaired-spin density (*43*, *44*). Line pairs 3′/3 and 5′/5 were assigned to the perpendicular and parallel hyperfine tensor components of the methyl protons at position 2 of P_B chlorophyll (Chl *a*). The line pair 4′/4 and 6′/6 are assigned to the 7-methyl protons, and the line pairs 7′/7 and 8′/8 are assigned to the 12-methyl protons (see Figure 1 for structure and numbering scheme). The data are summarized in Table 2. Except for the hfc's of the 7-methyl protons, the isotropic hfc's of $P_{700}^{+\bullet}$ in WT PS1 from *C. reinhardtii* are in good agreement with those reported by the Lubitz group (*16*). The hfc of the 12-methyl proton of the T739A mutant is significantly lower than that of WT (~0.53 MHz), while the hfc's of the methyl group protons at positions 2 and 7 did not display a significant change in magnitude. This effect is very similar to what was reported by Witt et al. (*16*), in which the 12-methyl hfc of $P_{700}^{+\bullet}$ in the T739V mutant (the most affected) was shifted down by ~0.47 MHz.

EPR Analysis of $^3P_{700}$. The $^3P_{700}$ state was generated by illumination at 5 K of thylakoid membranes containing PS1 with PhQs and all subsequent cofactors inactivated. This was accomplished by prior removal of the PsaC subunit (with urea) and double reduction of the PhQ(s) by illumination at 0 °C in the presence of dithionite (see Experimental Procedures for details). The EPR spectrum of $^3P_{700}$ in WT *Chlamydomonas* PS1 agreed very well with previous mea-

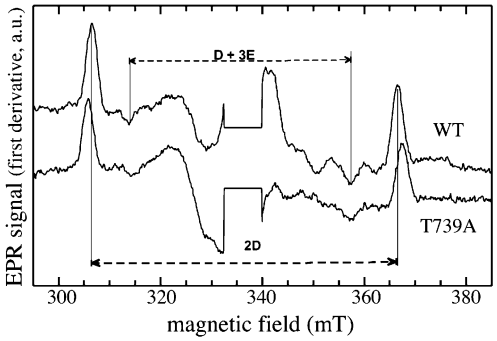

FIGURE 8: EPR spectra of $^3P_{700}$ in wild-type (upper) and mutant PsaA-T739A (lower). Conditions were $T = 4$ K, microwave power $= 60\ \mu$W, microwave frequency $= 9.44$ GHz, modulation amplitude $= 2.5$ mT, and modulation frequency $= 100$ kHz.

Table 3: Zero-Field Splitting Parameters of $^3P_{700}$ in WT PS1 and the PsaA-T739A Mutant

PS1	D (cm^{-1})	E (cm^{-1})
WT	0.0280	0.0042
PsaA-T739A	0.0288	0.0038

surements (*34*). The spectrum of $^3P_{700}$ in the mutant PsaA-T739A was significantly different from the WT spectrum (Figure 8); the zero-field splitting parameters derived from these spectra are listed in Table 3.

Directionality of Electron Transfer in PsaA-T739A. Recent analysis of electron transfer in *Chlamydomonas* PS1 mutants in vivo provided evidence that charge separation in PS1 can lead to reduction of either of the two PhQs, followed by subsequent electron transfer to the F_X iron−sulfur cluster (*9*). This observation seems to imply that electron transfer could proceed down either the A-branch or B-branch, leading to reduction of PhQ_A or PhQ_B, respectively. Since the H-bond to P_A seems to the most obvious source of asymmetry in P_{700}, we wondered whether removal of the H-bond would result in a redirection of electron transfer within PS1. We therefore examined the kinetics of PhQ^- reoxidation in the nanosecond regime by pump−probe laser-flash spectroscopy (*30*). The PsaA-T739A mutation had no detectable effect upon the rates or DAS of the two kinetic components assigned to PhQ^- reoxidation (Figure 9 and data not shown). This was expected, given the long distance between P_{700} and the phylloquinones. However, if the fraction of electrons delivered to one PhQ or the other became greater, we would expect the amplitude of the component assigned to reoxidation of that quinone to become larger. This expectation was not met. The relative amplitudes of the two components were not observably changed by the PsaA-T739A mutation (Figure 9). Thus, conversion of PsaA-Thr739 to alanine does not seem to cause a redirection of electron transfer within PS1.

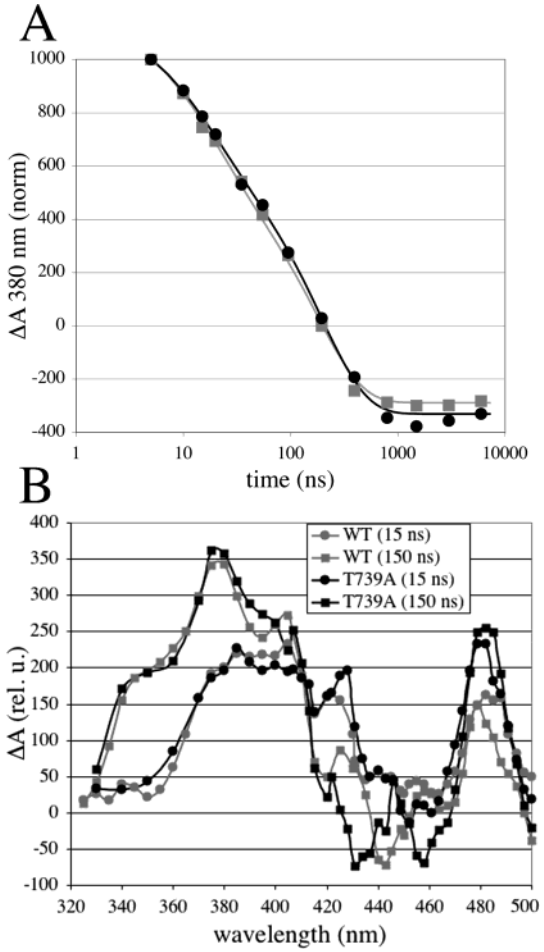

FIGURE 9: Panel A presents a semilog plot of the decay of absorbance at 380 nm in WT (gray) and the PsaA-T739A mutant (black) in the nanosecond time scale. Panel B presents the decay-associated spectra (DAS) in the nanosecond time scale in WT (gray) and the PsaA-T739A mutant (black). DAS for four kinetic decay components were calculated for each experiment: a 15-ns component (assigned to reoxidation of PhQ_B^-), a 150-ns component (assigned to reoxidation of PhQ_A^-), a component decaying with a time constant of $\sim 4\ \mu$s (assigned to rereduction of P_{700}^+), and a nondecaying component. The DAS of the 15-ns (circles) and 150-ns (squares) components are shown here. (The 4-μs DAS is shown in Figure 4B).

DISCUSSION

Summary of Results. Substitution of alanine for threonine at position 739 of PsaA was designed to remove the H-bond to the 13^1-keto oxygen of P_A and to make P_{700} more symmetric. Since this threonine accepts a H-bond from the H-bonded water molecule that is central to the H-bonding network, this mutation may disrupt the entire network. We also expected that the isomerization to Chl *a*′ might be inhibited in this mutant. We observed alteration of the P_{700} bleaching spectrum, several changes in the $P_{700}^+ - P_{700}$ FTIR difference spectrum, and a 60-mV decrease of the midpoint potential of P_{700}^+/P_{700}, testifying to significant perturbation of the environment of P_{700}. We note that these changes were of the same order of magnitude as the most severe mutations of the axial ligands to the magnesiums of the P_{700} Chls (*43*) and were at least as large and usually larger than the most severe of the substitution mutants in the same site (PsaA-T739V) reported by Witt et al. (*16*). However, we have no evidence that the mutation blocked incorporation of Chl *a*′ into the P_A site, nor did the ENDOR spectrum of P_{700}^+ in the mutant provide evidence for a large redistribution of unpaired spin to P_A. Finally, the mutation had no discernible effect upon the ability of PS1 to produce charge separation or upon the directionality of electron transfer within PS1. These effects are discussed in more detail below.

Presence of Chl a′. One of the unique features of P700 is that it is a heterodimer (Chl *a*/Chl *a*′). The "special pair" of type 2 reaction centers is made up of a dimer of the bulk

pigment: Chl *a* in the case of PS2, BChl *a* in the case of *R. sphaeroides* RC, etc. However, in the homodimeric type 1 RCs of *Chlorobium* and *Heliobacteria*, the corresponding pair seems to be composed of the 13^2 epimer of the bulk pigment: BChl *a*′ in the case of the chlorobial RC (*45*), and BChl *g*′ in the case of the heliobacterial RC (*46*). Since the RCs of these anoxygenic bacteria are homodimeric, they should have the same site for both members of the pair, thus forcing them to have the same chemical identity. Because PS1, the only known heterodimeric type 1 RC, can possess two different niches for the two pigments, it is uniquely capable of making a heterodimeric pair. The importance of the use of the 13^2 epimer in type 1 RCs, which seems to be used nowhere else in the organism, is still somewhat of a mystery. Moreover, the importance of a heterodimeric pair in PS1 has still not been adequately explained. We must note, however, that the results of our pigment extractions and HPLC analyses are inconsistent with loss of Chl *a*′ in the P_A site after mutation of PsaA-Thr739. This leads to a further mystery: if this H-bond is not responsible for isomerization of Chl *a* to Chl *a*′ or binding of Chl *a*′ at the P_A site, then what feature of PS1 *is* responsible for the chemical heterogeneity of P_{700}? Webber and Lubitz's proposal that the H-bond would catalyze isomerization by stabilizing an intermediate enolate form of Chl (*7*), although a very reasonable and appealing hypothesis, is not supported by these data. Whatever the driving force for incorporation of Chl *a*′ in the P_A site, it seems that a good deal of the asymmetry observed in P_{700} is due to this chemical heterogeneity and not to the asymmetry provided by the environment, an important feature of which is the H-bond from Thr739.

The Presence of a Hydrogen Bond to P_{700}. Do these data support the presence of a hydrogen bond between PsaA-Thr739 and the 13^1-keto group of P_A? Actually, this question should be addressed in terms of the three different states of P_{700} examined here: Does PsaA-Thr739 donate a H-bond the 13^1-keto group of P_A in the P_{700} ground state? In the oxidized (P_{700}^+) state? In the triplet ($^3P_{700}$) state?

We first consider the $P_{700}^+ - P_{700}$ optical difference spectra. The shape of these spectra for the PsaA-T739A mutant are very similar to those previously published for the T739H, T739Y, and T739V mutants (*16*). According to Witt et al. (*16*), the strength of the mutation was in the order (of increasing severity) tyrosine ≤ histidine < valine. In all of these, the major red bleaching band blue-shifted by almost the exact same amount. We note that the intensity of the minor bleaching band at ∼680 nm (compared to the major band at ∼690 nm) decreased somewhat with the severity of the mutation. In our PsaA-T739A spectrum, the ∼680-nm band is even less intense than that of the PsaA-T739V mutant. However, we have noticed that this band could be somewhat variable, and thus this difference might be artifactual. In addition, the secondary bleaching band at ∼442 nm was noticeably more intense in the PsaA-T739V mutant compared to the other two substitution mutants (*16*); the bleaching spectrum of PsaA-T739A shown here is almost identical to that of the PsaA-T739V mutant.

Although bleaching of the ground state absorption bands are not the only contributors to light-induced difference spectra, the fact that the mutation of PsaA-Thr739 alters the bleaching spectra of P_{700} argues for an effect upon the ground state. The main bleaching band at 700 nm (696 nm for *C. reinhardtii* P_{700}) is attributed to the low-energy band due to the coupling of P_A and P_B. Red shift of the Q_y transition relative to that found in monomeric Chl is thought to be due to the dimeric character of P_{700} (*47*, *48*). The fact that the main bleaching band blue-shifts in PsaA-T739A is consistent with either less coupling between P_A and P_B or with a decrease in the splitting between P_A and P_B. It is difficult to distinguish between these possibilities, because the high-energy exciton component cannot be observed reliably. However, if we assume that there is relatively little movement of P_A within its site after mutation of PsaA-Thr739, then it seems likely that the coupling will not be strongly affected. It is difficult to assess the strength of the H-bond directly from the effect of the mutation upon the bleaching spectrum. However, if we assume that the main effect upon the bleaching spectra is the loss of a H-bond, this would indicate that in all four of the mutants examined so far this H-bond is missing and that the minor differences may be due merely to environmental variability provoked by the different side chains.

The FTIR difference spectra should be able to indicate whether PsaA-Thr739 is H-bonded to the 13^1 keto C═O of P_A, However, interpretation of the FTIR difference spectra depends critically upon the assignment of the bands. There are two main hypotheses in the literature to link the H-bond to P_A with the bands observed in the FTIR DS. Breton and colleagues have assigned a negative band at ∼1639 cm^{-1} (in cyanobacterial PS1) to the 13^1-keto group of P_A, which upshifts to 1656 cm^{-1} upon cation formation (*8*). Such a low frequency for the C═O mode suggests that it is strongly H-bonded. In contrast, Hastings and co-workers suggested that the 1639(−)/1656(+) cm^{-1} difference band is due to imidazole mode(s) of the axial histidine ligand(s) of the P_{700} Chls (*26*). The large negative band at ∼1700 cm^{-1} was assigned to both 13^1-keto C═O groups in the ground state: P_B at 1703 cm^{-1} and P_A at 1694 cm^{-1}. In this interpretation, the P_B band upshifts by 14 cm^{-1}, and the P_A band downshifts by 10 cm^{-1} upon oxidation of P_{700} (*26*). This downshift after oxidation was interpreted in terms of a strengthening of the H-bond in the cation state. As shown in Figure 3, the FTIR difference spectra of the mutant and the wild-type are very different, and the negative band at 1639 cm^{-1} disappears in the mutant, and several bands are slightly up- or downshifted, compared to the bands in the WT spectrum. It is difficult to assess which model is correct, based on these data. However, we note that the 1639 cm^{-1} band does appear to shift in the mutant, as would be expected in Breton's model, although the position to which it shifts is not obvious. The main features in the FTIR DDS are a large increase in the positive band at 1689 cm^{-1} and a new negative band at 1672 cm^{-1}. A more involved discussion of the effect of the PsaA-T739A mutation upon the FTIR $P_{700}^+ - P_{700}$ difference spectrum has recently been published (*40*).

The assignment of the 1735(−)/1741(+) and 1748(−)/1754(+) cm^{-1} difference bands is less controversial. Both groups assigned these bands to the 13^3-ester carbonyls of P_A and P_B, respectively. The lower frequency band was assigned to the P_A 13^3-ester C═O, because this species probably interacts with the H-bond network. The fact that the 13^3-ester C═O bands of P_A and P_B (in the ground state) are unaltered by the mutation suggests that the water

molecule, and presumably the rest of the H-bond network, remains intact after loss of the PsaA-Thr739 side chain. Above we have suggested that the degree of upshift upon oxidation can be used as an indicator of pigment charge density. On the basis of this premise and a careful analysis of the bands in the WT and mutant spectra, we estimate that 14−18% of the positive charge density from P_B is shifted to P_A as a result of the T739A mutation.

There seems to be little question that there is a hydrogen bond to the 13^1-keto C═O of P_A in P_{700}^+. Both interpretations of the FTIR data invoke such a H-bond in the oxidized state. The main question is the strength of this bond, as discussed above. The ENDOR data are also consistent with the hypothesis that P_A is H-bonded in P_{700}^+, because of the shift of the hfc of the P_B 12-methyl upon mutation of PsaA-Thr739 to alanine. It is important to remember that the interpretation of strong localization of unpaired electron spin density on P_B implies that the resolved hfc's in the ^{1}H-ENDOR spectrum of P_{700}^+ are all assigned to P_B with the small peaks near ν_H attributed to the unresolved hfc's from P_A protons (*7*). Even though the PsaA-T739A mutation may affect a H-bond to the 13^1-keto group, which is close to the 12-methyl group and may change the spin density in this vicinity of P_A, this is *not* what was measured by this technique. Rather, the ENDOR results only provide information about the P_B side, since the spin density distribution of P_{700}^+ remains asymmetric in this mutant. Following this interpretation, the PsaA-T739A mutation results in a lower spin density at position 12 of P_B. This could be interpreted in terms of a redistribution of spin from P_B to P_A. However, it would have to be a very minor redistribution. A significant movement of spin from P_B to P_A would be expected to result in a decrease in *all* the hfc's of P_B and an increase in the hfc's of P_A, perhaps even enough to begin to resolve them. This was not observed. An alternate and nonexclusive interpretation would be that the mutation causes only an intramolecular redistribution of spin within P_B, without any transfer of spin to P_A. We favor the first hypothesis, which is more in line with the interpretation of the FTIR results in terms of a small transfer of positive charge from P_B to P_A in P_{700}^+, as discussed above. The reason a decrease of only the hfc of the 12-methyl group was observed is probably because this is the largest one resolved in the spectra, and it is thus easier to see alteration of this hfc. A similar effect was seen with the other PsaA-Thr739 mutants (*16*), although the shift in the hfc of the 12-methyl group was slightly larger with the PsaA-T739A mutant than with the PsaA-T739V mutant. It is likely that the mutation provokes both an intermolecular and an intramolecular redistribution of unpaired spin within P_{700}^+ and P_B.

The P_{700} oxidation potential will be strongly dependent upon the energy of both the ground and oxidized state of P_{700} and any changes to them induced by hydrogen bonding. The midpoint potential of P_{700}^+/P_{700} in the PsaA-T739A mutant is 60 mV below that of WT. This can be easily accommodated within the model proposed by Lubitz and co-workers for the electronic structure of P_{700} (*7*, *16*). The increased energy of the HOMO of P_A after loss of the H-bond would lead to a smaller energetic splitting between the energy levels of the super-MOs of P_{700}^+, an increase of the energy of the lower-energy super-MO, and a decrease of the energy of the higher-energy super-MO. This latter MO would contain the unpaired spin and would be repopulated upon reduction of P_{700}^+. An increase in its energy would make it more difficult to reduce, which is what we observed. Similar effects were observed in the purple bacterial RC after mutations were created to introduce H-bonds to the 13^1-keto groups of the BChls of P_{865} (*49*). In fact, introduction of a H-bond to either BChl caused a 60-mV increase in the midpoint potential, in striking agreement with our estimate of a 60-mV decrease upon loss of a H-bond. We note that this shift of −60 mV is significantly greater than that reported for the T739H (−9 mV), T739Y (−9 mV), and T739V (−32 mV) mutants (*16*). It is not clear why these shifts should be so different, if the H-bond is broken in all four cases, but small environmental changes and shifts of position within the dimer may explain this fact.

It seems likely that, if there is a hydrogen bond to P_A in the ground state, there will also be a hydrogen bond of similar strength in the triplet state ($^3P_{700}$). One expects much less structural change in the case of the triplet compared to the cation, because there is neither a change in the charge state of P_{700} nor the consequent structural relaxation of the protein medium in response to it. The mutation provoked a significant alteration of the EPR spectrum of $^3P_{700}$ (Figure 8 and Table 3). Interestingly, the direction and magnitude of the changes in the zero-field splitting parameters are very similar to what was previously observed in a mutant where the axial ligand to P_B (PsaB-His656) had been converted to leucine (*34*). This was interpreted in terms of a model in which the triplet was more localized. The corresponding change to the axial ligand of P_M in the purple bacterial reaction center resulted in replacement of bacteriochlorophyll with bacteriopheophytin and consequent localization of the triplet to the BChl half (*50*). Although it is not clear whether the PsaB-H656L mutation results in replacement of Chl with pheophytin, the severe perturbation of the properties of P_{700} in this mutant is consistent with this hypothesis (*18*, *34*, *43*, *51*). If this were the case, then one would expect localization of the triplet to P_A in the PsaB-H656L mutant. A similar argument might be made for PsaA-T739A mutant, since similar changes in the triplet EPR spectra were seen.

The localization of the triplet in $^3P_{700}$ is controversial. On the basis of the effects of axial ligand mutations upon the triplet−singlet difference spectra, Krabben et al. (*43*) concluded that the triplet was localized to P_B. However, this conclusion is not absolutely straightforward. First of all, although several mutations of the axial ligand to P_B were examined, only two mutations of the P_A axial ligand (to glutamine or serine) were studied in the triplet state. In both cases, the mutation to glutamine provoked no significant effect (*43*), so this relatively mild mutation was not informative. Thus, the only valid comparison was PsaB-H656S and PsaA-H676S. Both mutations induced a blue shift in the main bleaching band; this was expected, since this band is ascribed to the low-energy excitonic interaction, which is abolished by triplet formation. The crucial point was that a 670-nm positive band seemed to blue-shift ∼10 nm in the PsaB-H656S mutant, but a similar change was not seen in the PsaA-H676S mutant. However, interpretation of this effect hinges upon the assignment of this band, which was ascribed to changes in exitonic interactions between the triplet-bearing Chl and the neighboring accessory Chl (ec2). Thus, the mutation would identify P_B as the triplet-bearing Chl in $^3P_{700}$.

However, the positive band expected for the P_{700} Chl in the singlet ground state (i.e., not bearing the triplet) was not identified in the *Chlamydomonas* T-S spectrum. In spinach PS1, this is a weak band, despite the fact that it is expected to possess half the oscillator strength of the dimer, and is found at 682 nm (*52*). If the 670-nm positive band were instead assigned to this Chl, then the whole conclusion would turn around. Instead, one would conclude that P_B must be the Chl that does *not* bear the triplet. Although this interpretation seems less likely, it serves as a reminder that the conclusion that P_B bears the triplet is far from firm. Furthermore, FTIR $^3P_{700} - P_{700}$ difference spectra have been interpreted by Breton and co-workers (*8*) in terms of strong localization of the triplet on a Chl the 13^1-keto oxygen of which is strongly H-bonded, thus P_A. In the $^3P_{700} - P_{700}$ FTIR difference spectrum, the negative band at 1639 cm^{-1}, which they assign to the H-bonded 13^1-keto oxygen of P_A, shifts to 1594 cm^{-1} upon triplet formation. There is no contribution at 1700 cm^{-1} and thus no or very little triplet character on P_B. Thus, if one accepts the assignment of the 1639 cm^{-1} band to the 13^1-keto group of P_A, then the conclusion that P_A bears the triplet naturally follows. As discussed above, the interpretation of the $^3P_{700}$ EPR spectrum is not nearly so straightforward, but it would be consistent with such a proposal. It must be noted that Lubitz and co-workers implicitly accepted this premise when they used the assignment of the band at 1639 cm^{-1}, changes of which (in their $P_{700}^+ - P_{700}$ FTIR DS) they explained by changes in the strength of H-bonding to the 13^1-keto group of P_A (*16*), although they had previously contradicted it by assigning P_B as the main bearer of the triplet (*43*).

Spin and Charge Distribution in P_{700}^+. As mentioned above, the PsaA-T739A mutation appears to cause a small redistribution of spin and charge within P_{700}^+ from P_B to P_A. It should be noted that the spin and charge distributions will not be absolutely identical within an oxidized Chl. However, a redistribution of unpaired spin across the dimer should be accompanied by a similar redistribution of positive charge. ENDOR spectroscopy is sensitive to movements of unpaired spin both within a Chl and across the two Chls of P_{700}^+, while FTIR spectroscopy is exquisitely sensitive to the distribution of charge. As discussed above, the amount of redistribution of charge provoked by the loss of the H-bond is of the order of 14−18% as estimated by FTIR, and the results of ENDOR spectroscopy are in rough agreement with that in terms of unpaired spin.

The asymmetric environment of P_{700} has been touted as the underlying reason for the observed asymmetry of P_{700}^+. There are several differences between the P_A and P_B sites beyond the H-bond examined here. There is a tightly bound water molecule, which is part of a more extended H-bond network, and the possibility of H-bonds to the 13^2 and phytyl esters. However, the H-bond to the 13^1-keto group, which is part of the extended π-system of the Chl macrocycle would be expected to play the major environmental role in terms of causing asymmetry within the P_{700} dimer. Both the FTIR and ENDOR spectra agree that the effect of loss of the H-bond is relatively minor. This is in striking contrast to the effects of introducing H-bonds to the BChls of P865 in the purple bacterial RC. Introducing a H-bond to the 13^1-keto group of P_M shifted the P_L/P_M spin density distribution from 2.1 to 4.9, while a H-bond to P_L shifted it in the other direction to 0.9 (*53*). The downshift of hfc's of methyl protons of the H-bonded Chls and upshift of the nonbonded BChls were so complicated that TRIPLE analysis was required to follow them. Moreover, this spin density redistribution nicely correlated with charge redistribution as observed by FTIR (*54*). A recent study of the L-Arg135 and M-Arg164 mutants in the *R. sphaeroides* RC also showed a good correlation between charge density redistribution, as observed by FTIR, and spin density redistribution, as observed by ENDOR (*55*). In contrast, the ENDOR spectra of WT and the PsaA-T739A mutant in *C. reinhardtii* PS1 are almost superimposable, except for the modest downshift of the largest resolved hfc's. Thus, despite the fact that the H-bond to P_A seems to have a similar effect upon the oxidation potential of P_{700} as the introduced H-bonds did to P_{865} in the purple bacterial RC, it has a very small effect upon the spin density distribution as observed by ENDOR (Figure 7, Table 2) or upon the global **g**-tensor as seen by high-field EPR (Figure 6, Table 1). Thus, this H-bond does *not* explain the observed localization of unpaired spin in P_{700}^+. It is also unlikely that the other residues contributing to the H-bond network have a large role either, as recently observed with mutants in *Synechocystis* PCC6803 that target all of these residues simultaneously (Pantelidou, Konovalova, Chitnis, and Redding, manuscript in preparation). Instead, we suggest that the inherent chemical asymmetry of P_{700}, which has been largely unappreciated, is responsible for the observed functional asymmetry. As discussed above, we do not know why and how a Chl *a′* is inserted into the P_A site, even in the absence of PsaA-Thr739, but the fact that P_{700} is still a Chl *a′*/*a* heterodimer in the mutant likely explains why the spin of P_{700}^+ is also still localized to P_B.

To estimate the influence of this change of protein environment upon the electronic properties of P_{700}^+, we calculated isotropic hfc's of model complexes of the P_{700}^+ radical cation with the amino acid residues serving as H-bond donor (PsaA-Thr743) and axial ligands (PsaA-His680 and PsaB-His660), based upon the *T. elongatus* structure (see Experimental Procedures). We repeated this calculation after substituting the PsaA-Thr743 residue model with an alanine model in an effort to simulate the effect of the PsaA-T739A mutation in *Chlamydomonas*. In general, application of DFT for calculation of magnetic resonance parameters of large systems suffers from quantitative inaccuracy, but it can be quite successful in predicting general trends (*56*). We believe that the relative changes of hfc parameters in the WT vs T739A is such a trend that can be reasonably expected to be described by DFT. The calculated relative changes of isotropic hyperfine coupling constants for model complexes are compiled in Table 4, compared with the experimental data. There is reasonable agreement between the theoretical and experimental values. The calculations predict that, among the three methyl groups of P_B, only the hfc of the 12-methyl group would change significantly upon conversion of threonine to alanine and that it would decrease. This is precisely what was seen by ENDOR spectroscopy (Table 2). Moreover the extent of the predicted change was surprisingly close to the actual value. Very similar changes were calculated after substitution of threonine for glycine (data not shown), indicating that the major effect was the loss of the hydroxyl group.

Table 4: Calculated and Experimental Relative Changes of Methyl-Proton Isotropic hfc's in P_B of P_{700}^+ after Change of PsaA-Thr743 (739) to Alanine

	change in hfc (%) upon change of Thr → Ala	
position	calcd[a]	exptl[b]
2-methyl	−0.3	−1.4
7-methyl	+1.2	−0.9
12-methyl	−7.6	−9.9

[a] Isotropic hyperfine coupling constants were calculated for a model complex of P_{700}^+ radical cation with amino acid residues PsaA-Thr743, PsaA-His680, and PsaB−His660 and for the same complex after the threonine was converted to alanine (i.e., the hydroxyl and methyl groups were replaced with hydrogens). [b] Calculated from the data in Table 2.

Functional Consequences of Asymmetry within P_{700}. The Psa-T739A mutant is still phototrophic and has no obvious photochemical defect (data not shown). In fact, it is striking how little effect this mutation has upon the function of PS1, despite the significant changes to the spectroscopic properties of P_{700}. The asymmetry of P_{700} has been invoked as a reason that charge separation in PS1 should be unidirectional, as it is in the type 2 reaction centers. However, in *Chlamydomonas* PS1, it appears that electron transfer can proceed to both quinones of the two branches, followed by either a "slow" transfer (∼150 ns) from PhQ_A or a "fast" transfer (∼15 ns) from PhQ_B to F_X (*9*). Mutation of the PhQ_A site altered the slow kinetic component, while mutation of the PhQ_B site altered the fast kinetic component, but neither mutation affected the relative amplitudes of the two components (*9*). Here we used the ratio of these two phases as a measure of the relative use of the two branches. The PsaA-T739A mutant had no discernible effect upon directionality. It may be that the character of the excited state of the primary donor (P_{700}*) is unaffected by this mutation. None of the techniques used here probe the very short-lived P_{700}* state, so this supposition remains untested. However, the significant alterations of the ground-state spectra combined with the change in redox potential of the P_{700}/P_{700}^+ couple make likely a change in the redox potential of the P_{700}*/P_{700}^+ couple and consequently in the free energy change associated with charge separation.

Another possibility is that P_{700} is not, in fact, the primary electron donor. If instead primary charge separation generates an $ec2^+$ $ec3^-$ state, followed by rapid electron transfer from P_{700} to give the first observed charge-separated state, P_{700}^+ $ec3^-$, then asymmetry of P_{700}^+ would have nothing to do with directionality. However, it might play a role in rereduction of P_{700}^+ by the external electron donor—plastocyanin, in this case. We were surprised that the rate of rereduction of P_{700}^+ in vivo was not strongly affected by the PsaA-T739A mutation, given the 60-mV increase in midpoint potential. This rate is first-order, consistent with electron transfer within a preformed plastocynanin−PS1 complex. It may be that formation of this complex alters the midpoint potentials of the donor, acceptor or both, somewhat countering the effect of the mutation. However, a near-perfect correlation of the midpoint potential of P_{700}/P_{700}^+ measured in vitro and the in vivo rate of electron transfer from prebound plastocyanin to P_{700}^+ in WT and a set of P_{700} axial ligand mutants (*57*) make this explanation seem unlikely. This is an open question that requires further work.

ACKNOWLEDGMENT

We thank Jacqueline Girard-Bascou for providing the *P71* mutant.

REFERENCES

1. Crofts, A. R., and Wraight, C. A. (1983) The electrochemical domain of photosynthesis, *Biochim. Biophys. Acta 726*, 149−185.
2. Kirmaier, C., and Holten, D. (1987) Primary photochemistry of reaction centers from the photosynthetic purple bacteria, *Photosynth. Res. 13*, 225−260.
3. Jordan, P., Fromme, P., Witt, H. T., Klukas, O., Saenger, W., and Krauss, N. (2001) Three-dimensional structure of cyanobacterial photosystem I at 2.5 Å resolution, *Nature 411*, 909−917.
4. Fish, L. E., Kück, U., and Bogorad, L. (1985) Analysis of the two partially homologous P_{700} chlorophyll *a* proteins of maize photosystem I: Predictions based on the primary sequences and features shared by other chlorophyll proteins, *Molecular Biology of the Photosynthetic Apparatus*, pp 111−120, Cold Spring Harbor Laboratory, Cold Spring Harbor, NY.
5. Vallon, O., and Bogorad, L. (1993) Topological study of PSI-A and PSI−B, the large subunits of the photosystem-I reaction center, *Eur. J. Biochem. 214*, 907−915.
6. Golbeck, J. H., and Bryant, D. A. (1991) Photosystem I, in *Current Topics in Bioenergetics: Light Driven Reactions in Bioenergetics* (Lee, C. P., Ed.) pp 83−177, Academic Press, New York.
7. Webber, A. N., and Lubitz, W. (2001) P700: the primary electron donor of photosystem I, *Biochim. Biophys. Acta 1507*, 61−79.
8. Breton, J., Nabedryk, E., and Leibl, W. (1999) FTIR study of the primary electron donor of photosystem I (P700) revealing delocalization of the charge in $P700^+$ and localization of the triplet character in ^{3}P700, *Biochemistry 38*, 11585−11592.
9. Guergova-Kuras, M., Boudreaux, B., Joliot, A., Joliot, P., and Redding, K. (2001) Evidence for two active branches for electron transfer in photosystem I, *Proc. Natl. Acad. Sci. U.S.A. 98*, 4437−4442.
10. Brettel, K. (1988) Electron transfer from $A1^-$ to an iron−sulfur center with $t_{1/2}$ = 200 ns at room temperature in photosystem I. Characterization by flash absorption spectroscopy, *FEBS Lett. 239*, 93−98.
11. Bock, C. H., Van der Est, A. J., Brettel, K., and Stehlik, D. (1989) Nanosecond electron-transfer kinetics in photosystem I as obtained from transient EPR at room temperature, *FEBS Lett. 247*, 91−96.
12. Setif, P., and Brettel, K. (1993) Forward electron transfer from phylloquinone A1 to iron−sulfur centers in spinach photosystem I, *Biochemistry 32*, 7846−7854.
13. Brettel, K. (1998) Electron transfer from acceptor A1 to iron−sulfur clusters in photosystem I measured with a time resolution of 2 ns, in *Photosynthesis: Mechanisms and Effects* (Garab, G., Ed.) pp 611−614, Kluwer Academic Publishers, Dordrecht, The Netherlands.
14. Liebl, U., Mockensturm-Wilson, M., Trost, J. T., Brune, D. C., Blankenship, R. E., and Vermaas, W. (1993) Single core polypeptide in the reaction center of the photosynthetic bacterium *Heliobacillus mobilis*: structural implications and relations to other photosystems, *Proc. Natl. Acad. Sci. U.S.A. 90*, 7124−7128.
15. Büttner, M., Xie, D. L., Nelson, H., Pinther, W., Hauska, G., and Nelson, N. (1992) The photosystem I-like P840-reaction center of green S-bacteria is a homodimer, *Biochim. Biophys. Acta 1101*, 154−156.
16. Witt, H., Schlodder, E., Teutloff, C., Niklas, J., Bordignon, E., Carbonera, D., Kohler, S., Labahn, A., and Lubitz, W. (2002) Hydrogen bonding to P700: site-directed mutagenesis of threonine A739 of photosystem I in *Chlamydomonas reinhardtii*, *Biochemistry 41*, 8557−8569.
17. Picard, V., Ersdal-Badju, E., Lu, A., and Bock, S. C. (1994) A rapid and efficient one-tube PCR-based mutagenesis technique using *Pfu* DNA polymerase, *Nucleic Acids Res. 22*, 2587−2591.
18. Redding, K., MacMillan, F., Leibl, W., Brettel, K., Hanley, J., Rutherford, A. W., Breton, J., and Rochaix, J. D. (1998) A systematic survey of conserved histidines in the core subunits of Photosystem I by site-directed mutagenesis reveals the likely axial ligands of P700, *EMBO J. 17*, 50−60.
19. Bennoun, P., Spierer-Herz, M., Erickson, J., Girard-Bascou, J., Pierre, Y., Delosme, M., and Rochaix, J.-D. (1986) Characteriza-

tion of Photosystem II mutants of *Chlamydomonas reinhardtii* lacking the *psbA* gene, *Plant Mol. Biol. 6*, 151−160.
20. Boudreaux, B., MacMillan, F., Teutloff, C., Agalarov, R., Gu, F., Grimaldi, S., Bittl, R., Brettel, K., and Redding, K. (2001) Mutations in both sides of the photosystem I reaction center identify the phylloquinone observed by electron paramagnetic resonance spectroscopy, *J. Biol. Chem. 276*, 37299−37306.
21. Kuchka, M. R., Goldschmidt-Clermont, M., van Dillewijn, J., and Rochaix, J. D. (1989) Mutation at the *Chlamydomonas* nuclear NAC2 locus specifically affects stability of the chloroplast psbD transcript encoding polypeptide D2 of PS II, *Cell 58*, 869−876.
22. Harris, E. H. (1989) *The Chlamydomonas sourcebook. A comprehensive guide to biology and laboratory use*, Academic Press, San Diego, CA.
23. Fischer, N., Setif, P., and Rochaix, J. D. (1997) Targeted mutations in the psaC gene of *Chlamydomonas reinhardtii*: preferential reduction of F_B at low temperature is not accompanied by altered electron flow from photosystem I to ferredoxin, *Biochemistry 36*, 93−102.
24. Porra, R., Thompson, W., and Kriedemann, P. (1989) Determination of accurate extinction coefficients and simultaneous equations for assaying chlorophylls *a* and *b* with four different solvents: verification of the concentration of chlorophyll standards by atomic absorption spectroscopy, *Biochim. Biophys. Acta 975*, 384−394.
25. Nakamura, A., and Watanabe, T. (2001) Separation and determination of minor photosynthetic pigments by reversed-phase HPLC with minimal alteration of chlorophylls, *Anal. Sci. 17*, 503−508.
26. Hastings, G., Ramesh, V. M., Wang, R., Sivakumar, V., and Webber, A. (2001) Primary donor photooxidation in photosystem I: a reevaluation of ($P700^+$ − P700) Fourier transform infrared difference spectra, *Biochemistry 40*, 12943−12949.
27. Wang, R., Sivakumar, V., Johnson, T. W., and Hastings, G. (2004) FTIR difference spectroscopy in combination with isotope labeling for identification of the carbonyl modes of P700 and $P700^+$ in photosystem I, *Biophys. J. 86*, 1061−1073.
28. Baymann, F., and Rappaport, F. (1998) Electrostatic interactions at the donor side of the photosynthetic reaction center of *Rhodopseudomonas viridis*, *Biochemistry 37*, 15320−15326.
29. Béal, D., Rappaport, F., and Joliot, P. (1999) A new high-sensitivity 10-ns time-resolution spectrophotometric technique adapted to in vivo analysis of the photosynthetic apparatus, *Rev. Sci. Instrum. 70*, 202−207.
30. Joliot, P., and Joliot, A. (1999) In vivo analysis of the electron transfer within photosystem I: are the two phylloquinones involved? *Biochemistry 38*, 11130−11136.
31. Bratt, P. J., Rohrer, M., Krzystek, J., Evans, M. C. W., Brunel, L.-C., and Angerhofer, A. (1997) Submillimeter High-Field EPR Studies of the Primary Donor in Plant Photosystem I $P_{700}^{\bullet+}$, *J. Phys. Chem. B 101*, 9686−9689.
32. Parrett, K. G., Mehari, T., Warren, P. G., and Golbeck, J. H. (1989) Purification and properties of the intact P-700 and F_X-containing Photosystem I core protein, *Biochim. Biophys. Acta 973*, 324−332.
33. O'Malley, P. J., and Collins, S. J. (2001) The effect of axial Mg ligation on the geometry and spin density distribution of chlorophyll and bacteriochlorophyll cation free radical models: a density functional study, *J. Am. Chem. Soc. 123*, 11042−11046.
34. Redding, K., MacMillan, F., Leibl, W., Brettel, K., Rutherford, A. W., Breton, J., and Rochaix, J.-D. (1998) A survey of conserved histidines in the photosystem 1: Methodology and analysis of the PsaB−H656L mutant, in *Photosynthesis: Mechanisms and Effects* (Garab, G., Ed.) pp 591−594, Kluwer Academic Publishers, Dordrecht, The Netherlands.
35. Nakamura, A., Akai, M., Yoshida, E., Taki, T., and Watanabe, T. (2003) Reversed-phase HPLC determination of chlorophyll *a*′ and phylloquinone in Photosystem I of oxygenic photosynthetic organisms, *Eur. J. Biochem. 270*, 2446−2458.
36. Nakamura, A., Yoshida, E., Taki, T., and Watanabe, T. (2002) Universal existence of one chlorophyll *a*′ molecule in photosystem I of oxygenic photosynthetic organisms, *J. Photosci. 9*, 367−369.
37. Gibasiewicz, K., Ramesh, V., Lin, S., Redding, K., Woodbury, N., and Webber, A. (2001) Mutations of ligands to connecting chlorophylls perturbs excitation dynamics in the core antenna of PSI from *Chlamydomonas reinhardtii*, *PS2001 proceedings: 12th International Congress on Photosynthesis*, CSIRO Publishing, Brisbane, Australia.
38. Mantele, W. (1993) Reaction-induced infrared difference spectroscopy for the study of protein function and reaction mechanisms, *Trends Biochem. Sci. 18*, 197−202.
39. Nabedryk, E. (1996) Light-induced Fourier transform infrared difference spectroscopy of the primary electron donor in photosynthetic reaction centers, in *Infrared spectroscopy of biomolecules* (Mantsch, H., and Chapman, D., Eds.) pp 39−81, Wily-Liss, New York.
40. Wang, R., Sivakumar, V., Li, Y., Redding, K., and Hastings, G. (2003) Mutation induced modulation of hydrogen bonding to P700 studied using FTIR difference spectroscopy, *Biochemistry 42*, 9889−9897.
41. Webber, A. N., Su, H., Bingham, S. E., Kass, H., Krabben, L., Kuhn, M., Jordan, R., Schlodder, E., and Lubitz, W. (1996) Site-directed mutations affecting the spectroscopic characteristics and midpoint potential of the primary donor in photosystem I, *Biochemistry 35*, 12857−12863.
42. Watanabe, T., and Kobayashi, M. (1991) in *Chlorophylls* (Scheer, H., Ed.) pp 287−303, CRC Press, Boca Raton, FL.
43. Krabben, L., Schlodder, E., Jordan, R., Carbonera, D., Giacometti, G., Lee, H., Webber, A. N., and Lubitz, W. (2000) Influence of the axial ligands on the spectral properties of P700 of photosystem I: a study of site-directed mutants, *Biochemistry 39*, 13012−13025.
44. Käss, H., Fromme, P., Witt, H. T., and Lubitz, W. (2001) Orientation and electronic structure of the primary donor radical cation $P700^{+\bullet}$ in photosystem I: A single crystals EPR and ENDOR study, *J. Phys. Chem. B 105*, 1225−1239.
45. Hauska, G., Schoedl, T., Remigy, H., and Tsiotis, G. (2001) The reaction center of green sulfur bacteria, *Biochim. Biophys. Acta 1507*, 260−277.
46. Neerken, S., and Amesz, J. (2001) The antenna reaction center complex of heliobacteria: composition, energy conversion and electron transfer, *Biochim. Biophys. Acta 1507*, 278−290.
47. Schaffernicht, H., and Junge, W. (1982) Deconvolution of the red P700 difference spectrum based on a set of three Gaussian components: further evidence from literature spectrums, *Photochem. Photobiol. 36*, 111−115.
48. Schaffernicht, H., and Junge, W. (1981) Analysis of the complex band spectrum of P700 based on photoselection studies with photosystem I particles, *Photochem. Photobiol. 34*, 223−232.
49. Lin, X., Murchison, H. A., Nagarajan, V., Parson, W. W., Allen, J. P., and Williams, J. C. (1994) Specific alteration of the oxidation potential of the electron donor in reaction centers from *Rhodobacter sphaeroides*, *Proc. Natl. Acad. Sci. U.S.A. 91*, 10265−10269.
50. Bylina, E. J., Kolaczkowski, S. V., Norris, J. R., and Youvan, D. C. (1990) EPR characterization of genetically modified reaction centers of *Rhodobacter capsulatus*, *Biochemistry 29*, 6203−6210.
51. Leibl, W., Brettel, K., Nabedryk, E., Breton, J., Rochaix, J.-D., and Redding, K. (1998) Effect of PsaB-His656Leu mutation on optical and infrared difference spectra of P700 photooxidation, in *Photosynthesis: Mechanisms and Effects* (Garab, G., Ed.) pp 595−598, Kluwer Academic Publishers, Dordrecht, The Netherlands.
52. Carbonera, D., Collareta, P., and Giacometti, G. (1997) The P700 triplet state in an intact environment detected by ODMR A well resolved triplet minus singlet spectrum, *Biochim. Biophys. Acta 1322*, 115−128.
53. Rautter, J., Lendzian, F., Schulz, C., Fetsch, A., Kuhn, M., Lin, X., Williams, J. C., Allen, J. P., and Lubitz, W. (1995) ENDOR studies of the primary donor cation radical in mutant reaction centers of *Rhodobacter sphaeroides* with altered hydrogen-bond interactions, *Biochemistry 34*, 8130−8143.
54. Nabedryk, E., Allen, J. P., Taguchi, A. K., Williams, J. C., Woodbury, N. W., and Breton, J. (1993) Fourier transform infrared study of the primary electron donor in chromatophores of *Rhodobacter sphaeroides* with reaction centers genetically modified at residues M160 and L131, *Biochemistry 32*, 13879−13885.
55. Johnson, E. T., Mueh, F., Nabedryk, E., Williams, J. C., Allen, J. P., Lubitz, W., Breton, J., and Parson, W. W. (2002) Electronic and Vibronic Coupling of the Special Pair of Bacteriochlorophylls in Photosynthetic Reaction Centers from Wild-Type and Mutant Strains of Rhodobacter Sphaeroides, *J. Phys. Chem. B 106*, 11859−11869.
56. Fuchs, M. R., Schnegg, A., Plato, M., Schulz, C., Muh, F., Lubitz, W., and Mobius, K. (2003) The primary donor cation $P^{+\bullet}$ in

photosynthetic reaction centers of site-directed mutants of *Rhodobacter sphaeroides*: *g*-tensor shifts revealed by high-field EPR at 360 GHz/12.8 T, *Chem. Phys. 294*, 371−384.
57. Ramesh, V. M., Guergova-Kuras, M., Joliot, P., and Webber, A. N. (2002) Electron transfer from plastocyanin to the photosystem I reaction center in mutants with increased potential of the primary donor in *Chlamydomonas reinhardtii*, *Biochemistry 41*, 14652−14658.

BI036329P